ACS OMEGA

http://pubs.acs.org/journal/acsodf

Article

# Enhancing Tumor Accumulation and Cellular Uptake of Layered Double Hydroxide Nanoparticles by Coating/Detaching pH-Triggered Charge-Convertible Polymers

Tiefeng Xu,[‖] Jianping Liu,[‖] Luyao Sun, Run Zhang, Zhi Ping Xu,* and Qing Sun*

Cite This: *ACS Omega* 2021, 6, 3822−3830

Read Online

ACCESS | Metrics & More | Article Recommendations | Supporting Information

**ABSTRACT:** Layered double hydroxide (LDH) nanoparticles are extensively explored as multifunctional nanocarriers due to their versatility in both the host layer and the interlayer anion. In this study, we report modification of positively charged Cu-containing LDH nanoparticles with a pH-responsive charge-changeable polymer to improve the particle colloidal stability in blood circulation, reduce the nonspecific uptake by normal cells in organs, and subsequently facilitate tumor accumulation and uptake by tumor cells in the acidic tumor microenvironment. *In vitro* experimental results demonstrate that this promising charge-convertible polymer−LDH nanocarrier well reduces the capture by macrophages in the physiologic medium (pH 7.4) but facilitates the uptake by tumor cells due to detaching of the coated polymer layer in the weakly acidic condition (pH 6.8). Cu-containing LDH nanoparticles also show pH-responsive magnetic resonance imaging (MRI) contrast capacity (i.e., $r_1$ relaxivity). *In vivo* MRI further confirms effective tumor accumulation of the charge-convertible nanohybrids, with ∼4.8% of the injected dose accumulated at 24 h postintravenous injection, proving the potential as a versatile delivery nanocarrier to enhance the antitumor treatment.

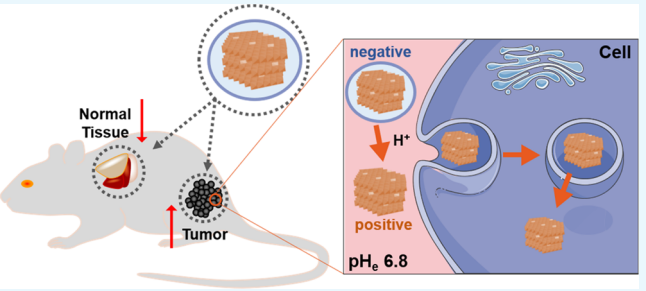


## INTRODUCTION

Two-dimensional (2D) nanomaterials have attracted tremendous attention in biomedical applications during the past decades due to the distinct physicochemical properties and excellent biocompatibility.[1−5] Especially, a larger number of investigations have been focused on layered double hydroxide (LDH) nanoparticles (NPs) for cancer diagnosis and therapy in view of various chemical compositions, facile preparation and isomorphic substitution, high loading capacity, tuneable size, and biodegradation.[6,7] This anionic clay material is represented with a general chemical formula $[M_{1-x}^{2+}M_{x}^{3+}(OH)_2](A^{n-})_{x/n}\cdot mH_2O$, where $M^{2+}$ is a divalent metal, $M^{3+}$ is a trivalent metal, and $A^{n-}$ is an anion. Each metal cation ($M^{2+}$ or $M^{3+}$) is octahedrally coordinated by six $OH^-$ anions and the adjacent octahedra ($M(OH)_6$) share edges to form a positively charged host layer. The interlayer anions ($A^{n-}$), as the counterion, hold the positive hydroxide layers together to form the layered structure.[8]

However, due to the interactions of various biomolecules in blood with the positive surface, LDH NPs readily aggregate in the physiological environment and serum, thus limiting their in vivo delivery, particularly tumor accumulation.[9,10] Therefore, the colloidal stability of LDH NPs has to be maintained in biological solutions, for which several surface functionalization approaches have been explored.[11,12] For example, Cao et al. constructed LDH NPs with phosphonic acid-terminated PEG to protect LDH from protein adsorption during blood circulation.[13] Enhanced circulation time allowed the PEGylated LDH NPs to accumulate in tumor tissues via the enhanced permeability and retention (EPR) effect. Our group has also developed a facile biocompatible approach to precoat and protect LDH NPs via electrostatic adsorption before intravenous injection, i.e., coating bovine serum albumin (BSA), a kind of natural biomolecule, on the LDH surface.[14] These two strategies effectively increase particle dispersion in culture medium, where BSA-coated LDH NPs have been demonstrated as a potent nanocarrier for therapeutics delivery. Other materials were also investigated to stabilize LDH in electrolyte media, such as silica,[15] Tween 80,[16] peroxidase enzyme,[17] liposomes,[18] lipids,[19] polymers,[20] and polyelectrolytes.[21,22] It is true that these surface engineering methods enhance the colloidal stability of LDH NPs and extend their blood circulation and tumor accumulation. However, they either require tedious modification processes (such as silica coating) or change the surface property of LDH NPs (such as

Received: November 12, 2020
Accepted: January 12, 2021
Published: January 27, 2021

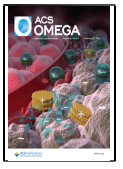

the charge from positive to negative). It is known that neutrally PEGylated nanoparticles and negatively charged material-coated LDH NPs do not easily enter cancer cells for therapy because of electrostatic repulsion with the negatively charged cell membrane,[23] thus reducing the antitumor efficacy even though these modified LDH NPs efficiently accumulate in the tumor tissues.

To solve this dilemma issue, we designed a pH-sensitive charge-convertible LDH-based nanoplatform, which hides the LDH-positive surface in the normal physiological environment but re-exposes the positive surface of LDH nanoparticles once accumulated in the tumor tissue, as schematically shown in Scheme 1. The charge-convertible property of LDH-based nanoplatform was achieved by complexing LDH with a negatively charged polymer (PAMA/DMMA) via electrostatic interactions. PAMA/DMMA is a dimethylmaleic acid (DMMA)-modified poly(2-aminoethyl methacrylate hydrochloride) polymer (Scheme S1). In the slightly acidic tumor microenvironment (TME), DMMA hydrolysis makes the negatively charged polymer to transform into the positive one (Scheme S1), and thus, the hydrolyzed polymer detaches from the positively charged LDH surface because of electrostatic repulsion, re-exposing the naked LDH in TME (Scheme 1). The naked LDH nanoparticles can easily interact with negatively charged cell membranes and quickly enter the cells via clathrin-mediated endocytosis.[24] To verify the advantage of PAMA/DMMA coating in tumor accumulation and subsequent cellular uptake, copper (Cu) was introduced into the LDH hydroxide layer (Cu-LDH) as the tumor MRI contrast agent and the probe for particle biodistribution detection and fluorescein isothiocyanate (FITC) in the interlayer as the uptake marker. In this research, the charge conversion of Cu-LDH@PAMA/DMMA NPs was verified in pH 6.8 buffer, which enhanced the cellular uptake. Moreover, the tumor accumulation of Cu-LDH@PAMA/DMMA NPs was also significantly improved in comparison with reported data in similar conditions.

**Scheme 1. Illustration of Negatively Charged Cu-LDH@PAMA/DMMA Accumulation in the Tumor Tissue and Subsequent Detachment of the Polymer in TME for Enhanced uptake by Tumor Cells**[a]

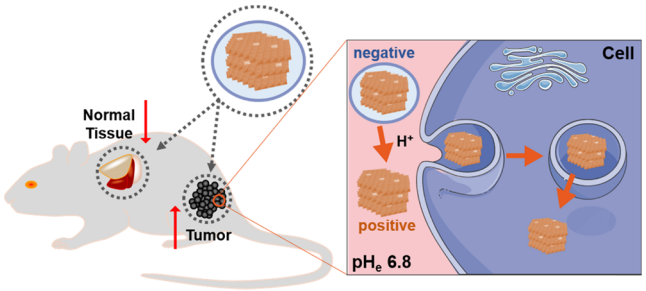


[a]$pH_e$, extracellular pH.

## RESULTS AND DISCUSSION

**Physicochemical Features of PAMA/DMMA-Modified Cu-LDH NPs.** The pH-responsive PAMA/DMMA polymer was prepared in a two-step procedure (Scheme S2). Briefly, the positively charged PAMA polymer was first synthesized via atom-transfer radical polymerization (ATRP).[25] Then, the terminated amino group in PAMA reacted with the carboxylate group in DMMA to reverse the polymer charge from positive to negative in a physiological solution. Measured in a gel permeation chromatography (GPC) system (Table S1), the degrees of polymerization (DP) of PAMA and DMMA were ~28 and ~18, respectively, implying that approximately 64% of amino groups in PAMA was successfully conjugated with DMMA. The narrow molecular weight distribution ($M_w/M_n$) (PDI = 1.06) and the structure of PAMA/DMMA were also

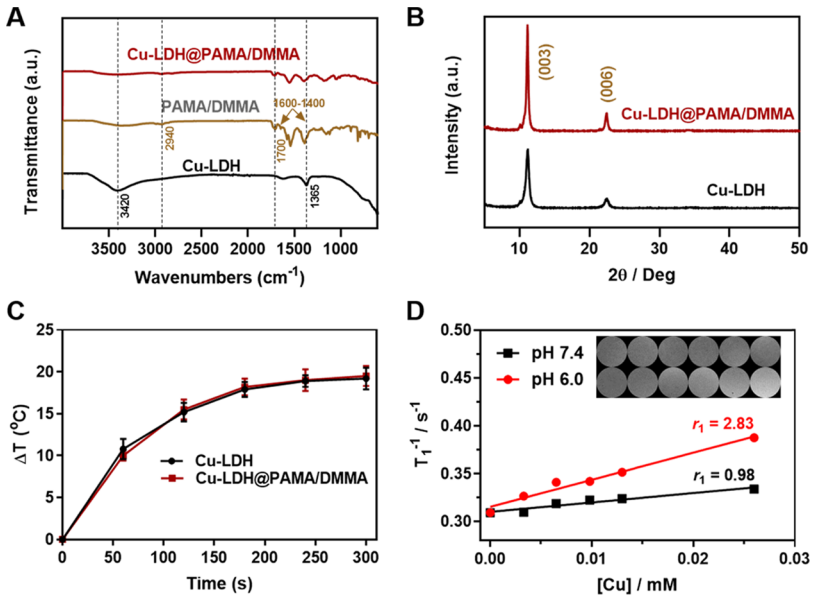


**Figure 1.** Characteristics of Cu-LDH@PAMA/DMMA hybrid NPs. (A) FT-IR spectra and (B) XRD patterns of Cu-LDH@PAMA/DMMA and Cu-LDH NPs. (C) Temperature profiles of Cu-LDH and Cu-LDH@PAMA/DMMA suspensions ([Cu] = 125 $\mu$g/mL) upon 808 nm laser irradiation (1.0 W/cm$^2$, 5 min). (D) Plot of $1/T_1$ versus Cu concentration to determine the $T_1$ relaxivity ($r_1$) of Cu-LDH NPs in buffers with pH 7.4 and 6.0. Inset: $T_1$-weighted MR images of Cu-LDH NPs in pH 7.4 and 6.0 buffers.


https://dx.doi.org/10.1021/acsomega.0c05520
ACS Omega 2021, 6, 3822−3830

confirmed with the GPC measurement and $^1$H NMR spectrum, respectively (Table S1 and Figure S1).

Subsequently, the carboxylate-terminated ($-COO^-$) PAMA/DMMA polymer was coated onto the surface of positively charged Cu-LDH via electrostatic interactions in the Cu-LDH suspension to endow Cu-LDH nanoparticles (NPs) with a charge-convertible character in response to acidity in the tumor extracellular environment. Pristine Cu-LDH NPs had an average particle size of 39.4 nm with a $\zeta$-potential of 33.7 mV (Table S2). As also listed in Table S2, Cu-LDH@PAMA/DMMA NPs were poorly dispersed in water with polydispersity indexes (PDI) of 0.412 and 0.373 at the polymer/LDH mass ratios of 0.2:1 and 0.5:1, possibly resulting from the insufficient amount of polymer for coating. When the mass ratio of the polymer to Cu-LDH was increased from 1:1 to 5:1, the nanosystems were fully coated and well suspended in water, as confirmed by the average size similar to pristine Cu-LDH (51−54 nm at 3:1−5:1 vs 39 nm of Cu-LDH) and the small PDI (0.112−0.126 at 3:1−5:1). Moreover, the reduced surface charge (for example, −25.6 to −26.6 mV at 3:1−5:1) demonstrated successful adherence of the pH-responsive negatively charged polymer onto positively charged LDH nanoparticles (33.7 mV). Thus, we chose 3:1 of the polymer to Cu-LDH mass ratio for surface modification in the following experiments, considering the particle dispersity (smaller size) and the polymer coating efficiency (less PAMA/DMMA used).

Fourier transform infrared (FT-IR) spectra of Cu-LDH, PAMA/DMMA, and Cu-LDH@PAMA/DMMA powders are shown in Figure 1A. Two characteristic bands centered at 1365 and 3420 $cm^{-1}$ were found in Cu-LDH, corresponding to $CO_3^{2-}$ contamination and O−H bonds in LDH host layers, respectively. The spectrum of the PAMA/DMMA polymer had strong peaks at 2940 $cm^{-1}$, assigned to the asymmetrical stretching vibration of saturated $CH_2$ groups, and peaks at 1700 $cm^{-1}$ to C═O, assigned to stretching vibration in the −COOH group. Another two intense absorption peaks in the range of 1600−1400 $cm^{-1}$ can be attributed to the vibrations of C═O and C−O in −COO− groups of the polymer that are attached on the LDH nanoparticle surface. As expected, these typical peaks were clearly observed in Cu-LDH@PAMA/DMMA nanohybrids, indicating the successful modification of Cu-LDH NPs with the PAMA/DMMA polymer. Quantitatively, 66−71 wt % of PAMA/DMMA in Cu-LDH@PAMA/DMMA was calculated based on the data of thermogravimetry analysis (TGA) and CHN elemental analysis (EA) (Table S3), revealing that about 70% of the added polymer was coated on Cu-LDH nanoparticles at the polymer/LDH mass ratio of 3:1. In addition, the powder X-ray diffraction (XRD) pattern of Cu-LDH@PAMA/DMMA shows typical (003) and (006) diffractions, similar to that of pristine LDH NPs (Figure 1B), indicating that surface coating with PAMA/DMMA does not affect the crystallinity of the Cu-LDH phase.

Cu incorporation enables MgAl-LDH-based nanoparticles to absorb and transform 808 nm NIR light into thermal energy (Figures S2 and S3). A distinct photothermal conversion in the Cu-LDH suspension at [Cu] = 125 $\mu$g/mL was observed in infrared thermal images (Figure S3). Moreover, the photostability of Cu-LDH NPs was well kept in a five-continuous "irradiation−cooling" process (Figure S4). Quantitatively, the photothermal transduction efficiency ($\eta$) of Cu-LDH NPs was estimated as 50.5%, based on the 300 s natural cooling profile (Figure S5). The photothermal conversion of Cu-LDH@PAMA/DMMA upon 808 nm laser irradiation was also monitored. Cu-LDH@PAMA/DMMA exhibited a temperature profile similar to that of pristine Cu-LDH, both increasing the suspension temperature by ∼19 °C at [Cu] = 125 $\mu$g/mL upon NIR irradiation at 1.0 W/$cm^2$ for 5 min (Figure 1C), indicating that the polymer coating does not reduce the photothermal conversion efficiency of Cu-LDH NPs.

The $T_1$-weighted MR imaging of Cu-LDH NPs was concentration-dependent (Figure 1D, inset). The corresponding longitudinal relaxivity ($r_1$) of Cu-LDH NPs was calculated to be 0.98 $mM^{-1}$ $s^{-1}$ in PBS (pH 7.4), comparable to those of CuS (0.12, 0.26 $mM^{-1}$ $s^{-1}$), $Cu_3P$ (0.59 $mM^{-1}$ $s^{-1}$), CuO (0.38 $mM^{-1}$ $s^{-1}$), and other Cu-based nanoparticles (Table S4).[26−29] Significantly, $r_1$ increased to 2.83 $mM^{-1}$ $s^{-1}$ in pH 6.0 buffer, similarly to the previous report.[30] Here, the weak acidity significantly enhanced the MRI contrast capacity, which will be very useful for the diagnosis of tumors via the pH-sensitive MR images, as presented shortly for in vivo studies.

Naked LDH nanoparticles are severely aggregated in PBS and culture medium due to adsorption of ions and serum proteins on the LDH surface, which leads to reduction of the electrostatic repulsion and aggregation.[14] Colloidal stability of Cu-LDH@PAMA/DMMA in electrolyte solution was simulated by monitoring the hydrodynamic particle size in PBS (pH 7.4) and Dulbecco's modified Eagle's medium (DMEM) with 10% FBS for 72 h (Figure S6). No aggregation was observed at different time points in PBS, while Cu-LDH@PAMA/DMMA NPs (40−50 nm) seemed to slightly aggregate into 100 nm particles in DMEM with 10% FBS, probably due to the bridging effect of proteins between two LDH nanoparticles.[14] Clearly, the negatively charged PAMA/DMMA helps retain the colloidal stability of Cu-LDH NPs and small aggregates in the physiological environment for 72 h, which may assist prolong blood circulation and enhance accumulation in the tumor tissue.

**Charge-Convertible Property of Cu-LDH@PAMA/DMMA.** PAMA/DMMA contains a pH-responsive amide linker, which is stable in normal physiological conditions but rapidly hydrolyzes once in a mildly acidic environment[31] to expose positively charged amino groups (Scheme S1). Subsequently, electrostatic repulsion between both positively charged amino groups in PAMA and the positively charged surface of Cu-LDH leads two entities to separate, as verified by the change of the average particle size, the $\zeta$-potential, and morphology of Cu-LDH@PAMA/DMMA in solutions with pH 7.4 and 6.8. As shown in Figure 2A, the average particle size of Cu-LDH@PAMA/DMMA was around 45 nm in the pH 7.4 solution, which decreased to 38 nm in pH 6.8 buffer, similar to that of pristine Cu-LDH (39 nm) (Table S2). More obviously, the $\zeta$-potential of Cu-LDH@PAMA/DMMA was −26 mV at pH 7.4, while it was converted to +29 mV after incubation in pH 6.8 buffer for 2 h (Figure 2A). Moreover, dynamic monitoring of the $\zeta$-potential of Cu-LDH@PAMA/DMMA NPs in pH 6.8 buffer showed that the negative $\zeta$-potential of Cu-LDH@PAMA/DMMA NPs was gradually reversed to a positive one and reached +30 mV within 60 min, while the negative $\zeta$-potential (−24 mV) was kept unchanged during incubation in the pH 7.4 solution (Figure 2B). The charge conversion and the size decrease of Cu-LDH@PAMA/DMMA with the buffer pH changing from 7.4 to 6.8 reveal that pH-sensitive PAMA/DMMA was peeled off from the surface of Cu-LDH@PAMA/DMMA, re-exposing pristine positively charged Cu-LDH NPs.


https://dx.doi.org/10.1021/acsomega.0c05520
ACS Omega 2021, 6, 3822−3830

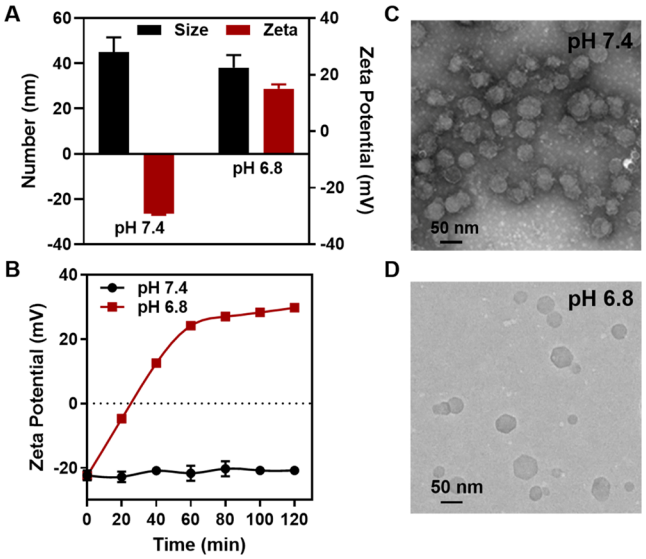


**Figure 2.** pH-responsive charge conversion of Cu-LDH@PAMA/DMMA when the buffer pH changing from 7.4 to 6.8. (A) DLS size and ζ-potential after incubation in the buffer for 2 h. (B) Dynamic ζ-potential changes in two buffers; transmission electron microscopy (TEM) images of Cu-LDH@PAMA/DMMA incubated in the buffers with pH 7.4 (C) and 6.8 (D) for 2 h.

The detachment of the polymer from the Cu-LDH surface was also visualized in transmission electron microscopy (TEM) images. As shown in Figure 2C, most hexagonal and platelike LDH NPs in pH 7.4 buffer were obviously surrounded by a dark ring, i.e., phosphotungstic acid-stained PAMA that was coated on the surface of Cu-LDH NPs. In contrast, the dark ring disappeared from the Cu-LDH NP surface after 2 h incubation in pH 6.8 buffer (Figure 2D), demonstrating successful separation of the polymer from Cu-LDH NPs. These observations together corroborate that the PAMA/DMMA polymer layer was detached from the Cu-LDH@PAMA/DMMA surface in response to weak acidity, reversing the particle surface charges from negative to positive.

**Charge Conversion-Enhanced Cellular Internalization and Photothermal Apoptosis.** In the physiological condition (pH 7.4), negatively charged Cu-LDH@PAMA/DMMA nanoparticles may be less efficiently internalized by normal cells (such as less capture by macrophages during circulation) to minimize adverse effects, thanks to electrostatic repulsions with the negatively charged cell membrane. Once the nanosystem accumulates in tumor tissues, the acidic extracellular environment (pH 6.5−6.8) hydrolyzes the pH-responsive PAMA/DMMA polymer and re-exposes positively charged pristine Cu-LDH NPs, which helps adhere onto the negatively charged cytomembranes for enhanced cellular uptake. To verify this hypothesis, fluorescein isothiocyanate (FITC) was intercalated into the Cu-LDH interlayer to investigate FITC/Cu-LDH@PAMA/DMMA cellular uptake by normal cells (macrophages, Raw 264.7) and cancer cells (B16F0).[14]

Time-dependent cellular uptake of Raw 264.7 and B16F0 cells via flow cytometry analysis shows that Cu-LDH@PAMA/DMMA nanoparticles were internalized in cells after 2−4 h incubation (Figure S7). As shown in confocal laser scanning microscopy (CLSM) images (Figure 3A,B), macrophages (Raw 264.7) incubated with FITC/Cu-LDH@PAMA/DMMA NPs for 4 h in pH 7.4 medium displayed very weak intracellular green signals, while much stronger fluorescence emission was observed in pH 6.8 medium. A similar phenomenon was also observed in B16F0 cancer cells. When the medium pH decreased from 7.4 to 6.8, the green fluorescence intensity was significantly increased, indicating that much more FITC/Cu-LDH NPs were internalized by B16F0 cells in pH 6.8 medium. Based on the flow cytometry analysis, the fluorescence intensity of macrophages incubated in pH 7.4 medium was only one-third of that in pH 6.8 medium, and the fluorescence intensity of B16F0 cells incubated in pH 6.8 culture medium was 5 times that in pH 7.4 culture medium (Figure 3C). The significant enhancement

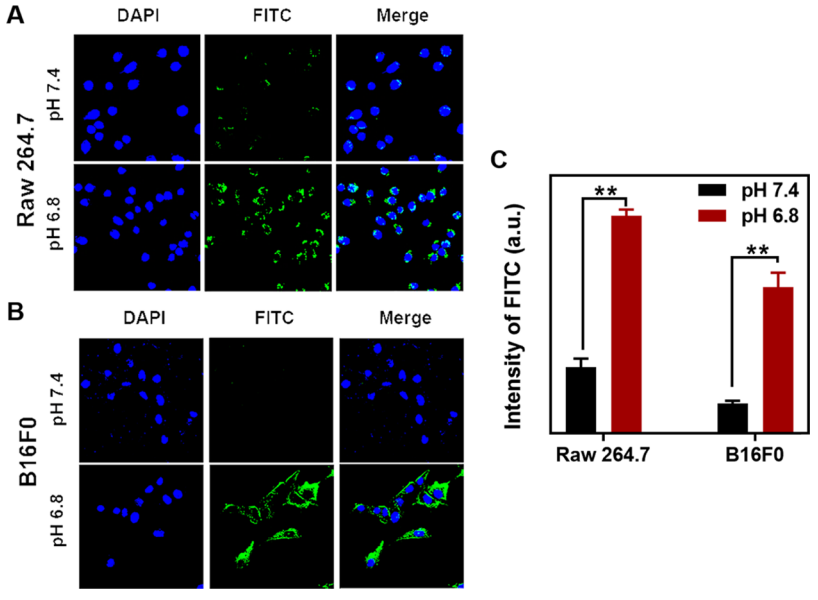


**Figure 3.** Uptake of Cu-LDH@PAMA/DMMA by B16F0 and Raw 264.7 cells. CLSM images of Raw 264.7 cells (A) and B16F0 cancer cells (B) and their mean fluorescence intensity (C) via flow cytometric analysis after the cells were treated with Cu-LDH@PAMA/DMMA in media with pH 7.4 and 6.8 at 37 °C for 4 h. $^{**}p < 0.01$.



https://dx.doi.org/10.1021/acsomega.0c05520
ACS Omega 2021, 6, 3822−3830

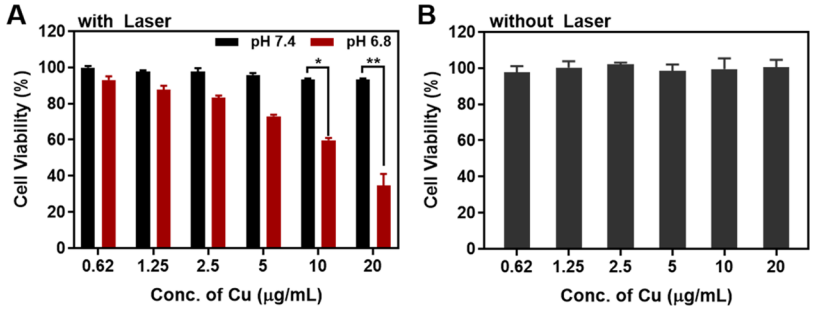


**Figure 4.** Cytotoxicity evaluation of Cu-LDH@PAMA/DMMA. (A) Cell viability of Cu-LDH@PAMA/DMMA after 20 h incubation in pH 7.4 and 6.8 media, washing away of Cu-LDH NPs, subsequent 808 nm laser irradiation (1 W/cm$^2$, 3 min), and another 4 h incubation in normal media. *$p$ <0.05, **$p$ <0.01. (B) Cell viability of Cu-LDH@PAMA/DMMA after 24 h incubation in pH 7.4 media, without laser irradiation.

of cellular uptake with the medium pH changing from 7.4 to 6.8 thus confirms that Cu-LDH NPs coated with negatively charged polymer prevents their uptake by normal cells in the physiological environment (pH 7.4), which may reduce undesirable cellular uptake and consequent side effects during blood circulation. When the coating layer is peeled off in the acidic environment (pH 6.8, such as in TME), positively charged Cu-LDH NPs are exposed, facilitating uptake by cancer cells and improving therapeutic efficacy.

Interestingly, 808 nm laser irradiation resulted in obvious inhibition of cell proliferation in a dose-dependent manner in pH 6.8 medium (Figure 4A), in sharp contrast to the case in pH 7.4 medium. For example, the cell viability decreased to 60% and 35% after incubation in pH 6.8 medium at [Cu] = 10 and 20 $\mu$g/mL, respectively, for 20 h, washing away of Cu-LDH NPs, subsequent 808 nm laser irradiation at 1 W/cm$^2$ for 3 min and another 4 h incubation in standard medium. However, the cell viability was kept at 90−95% in pH 7.4 medium under the same conditions, implying a much smaller amount of Cu-LDH NPs taken up by cancer cells. This contrast can be well explained by the difference in cellular uptake efficiency in neutral and acidic conditions (Figure 3B,C).

It is also worth mentioning that Cu-LDH@PAMA/DMMA showed almost no cytotoxicity to B16F0 cancer cells after incubation for 24 h in pH 7.4 medium at the copper concentration of up to 20 $\mu$g/mL (i.e., ∼140 $\mu$g/mL Cu-LDH and ∼300 $\mu$g/mL PAMA/DMMA) without laser irradiation (Figure 4B).

**Enhanced Tumor Accumulation in the Animal Model.** As mentioned previously, the negatively charged PAMA/DMMA polymer coating may reduce the clearance of positively charged Cu-LDH nanoparticles in blood circulation. The prolonged circulating lifetime may then increase the chance for Cu-LDH@PAMA/DMMA NPs to extravasate through vascular fenestrations and accumulate in the tumor tissue. To confirm the hypothesis, sequential MR images were recorded to dynamically monitor the tumor accumulation of Cu-LDH@PAMA/DMMA NPs, as Cu-LDH owned a $r_1$ relaxivity of 2.83 mM$^{-1}$ s$^{-1}$ in pH 6.0 medium (Figure 1D) as well as 2.75 mM$^{-1}$ s$^{-1}$ in pH 6.5 buffer, a clear contrast to that in the pH 7.4 physiological solution.[30] As shown in Figure 5A, $T_1$-weighted MR signal brightness around the tumor tissue enhanced gradually and reached an apex at 24 h post iv injection of Cu-LDH@PAMA/DMMA NPs, followed by the brightness weakening until 72 h. Corresponding signal intensities (Figure 5B) confirmed the time-dependent accumulation in the first 24 h postinjection, with the relative

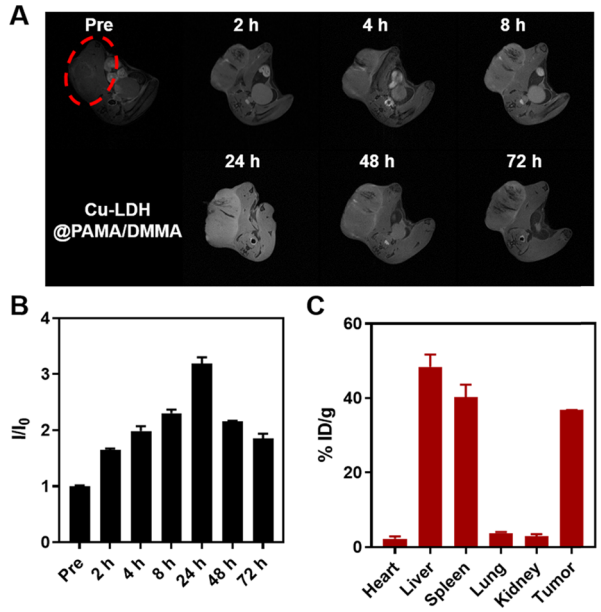


**Figure 5.** Tumor accumulation of Cu-LDH@PAMA/DMMA. (A) *In vivo* $T_1$-weighed MR images of B16F0 tumor-bearing mice in a time-course before and after intravenous injection of Cu-LDH@PAMA/DMMA within 72 h. (B) Corresponding relative signal intensity in tumors. $I_0$ and $I$: MRI signal intensity of the tumors before injection and at a specific time point postinjection, respectively. (C) Cu amount in the heart, liver, spleen, lung, kidney, and tumor dissected from mice at 24 h postinjection, determined by inductively coupled plasma-optical emission spectrometry (ICP-MS).

intensity at 24 h being increased from 1.0 to 3.2. This MRI intensity increase is ascribed to continuous infiltration of Cu-LDH@PAMA/DMMA NPs into the tumor tissue via enhanced permeability and retention (EPR) effect and re-exposure of Cu-LDH after detachment of the coated polymer due to weak acidity (pH 6.5−6.8), leading to a much stronger MRI contrast at 24 h postinjection in comparison with that in the blood (pH 7.4). Subsequently, MR signals decreased due to NP biodegradation in the acidic tumor microenvironment, while considerable signals (1.8) were still detected even at 72 h postinjection, meaning that there were some Cu-LDH residuals left.[30]

Semiquantitatively, the Cu level in major organs was assessed at 24 h post iv injection via ICP-MS to examine the biodistribution of charge-convertible Cu-LDH@PAMA/DMMA NPs in the B16F0-bearing mouse model. As shown in Figure 5C, around ∼37% ID/g of injected Cu dose


https://dx.doi.org/10.1021/acsomega.0c05520
ACS Omega 2021, 6, 3822−3830

Table 1. Comparison of the Cu Level in Tumors, Liver, and Spleen at 24 h Post iv Injection of Cu-LDH Nanoparticles Formulated with Charge-Convertible (PAMA/DMMA and PEG-PA/DM) and Noncharge Convertible (BSA) Polymers

| surface | LDH | tumor | | liver | spleen |
|---|---|---|---|---|---|
| charge-convertible polymer | Cu-LDH @PAMA/DMMA | % ID | 4.8 | | |
| | | % ID/g | 37 | 48 (0.77)[a] | 40 (0.92)[a] |
| | Cu-LDH @PEG-PA/DM (Liu et al.[32]) | % ID/g | 6.0 | | |
| | | % ID/g | 47 | 48 (0.98) | 45 (1.04) |
| BSA | Cu-LDH@BSA (Liu et al.[32]) | % ID | 3.0 | | |
| | | % ID/g | 15 | 59 (0.25) | 85 (0.18) |
| | Cu-LDH@BSA (Li et al.[30]) | % ID | 3.6 | | |
| | | % ID/g | 6.4 | 47 (0.14) | 15 (0.43) |
| | Cu-LDH@BSA (Shi et al.[33]) | % ID | | | |
| | | % ID/g | 6.8 | 24 (0.28) | 12 (0.57) |
| others | Cy5.5-IPA/LDH (Gao et al.[34]) | % ID | | | |
| | | % ID/g | 24 | 15 (1.60) | 2 (12.00) |
| | 5-FU/LDH (Choi et al.[35]) | % ID | | | |
| | | % ID/g | 33 | 12 (2.75) | 8 (4.12) |
| | LDH@PLGA (Ray et al.[20]) | % ID | | | |
| | | % ID/g | 20.7 | 16.4 (1.26) | 20.7 (1.00) |

[a]The value in the parentheses is the ratio of % ID/g in tumor to that in the liver or spleen.

accumulated in the tumor tissue, comparable to that using similar charge-convertible Cu-LDH@PEG-PA/DM (~48% ID/g) but much higher than Cu-LDH@BSA (~7-15% ID/g) in previous reports,[30,32,33] as summarized in Table 1. Correspondingly, the amount of Cu-LDH accumulated in the tumor tissue at 24 h post iv injection was 4.8% of the total injected dose (4.8% ID) of Cu-LDH@PAMA/DMMA NPs, also comparable to that of Cu-LDH@PEG-PA/DM (~6.0% ID) but much higher than Cu-LDH@BSA (3.0-3.6% ID) reported previously.

On the other hand, the liver and spleen nearly captured the rest Cu-LDH@PAMA/DMMA NPs, with ~48% and ~40% ID/g, respectively (Figure 5C). This biodistribution is similar to that in previous reports, as summarized in Table 1. These data demonstrate that the liver and spleen clear up most Cu-LDH NPs no matter whether these NPs are coated with the charge-convertible polymer (PAMA/DMMA or PEG-PA/DM) or noncharge convertible polymer (BSA). This is clearly reflected by the ratio of %ID/g in tumor to that in the liver and spleen. These ratios were 0.14−0.28 and 0.18−0.57, respectively, for BSA-coated Cu-LDH NPs (Table 1). In contrast, these ratios increased to 0.77−0.98 and 0.92−1.04, respectively, for Cu-LDH NPs coated with the charge-convertible polymer (PAMA/DMMA or PEG-PA/DM). The ratio increase clearly indicates that much more charge-convertible polymer-coated Cu-LDH NPs accumulate in the tumor tissue than noncharge convertible BSA-coated Cu-LDH NPs. In comparison with PAMA/DMMA, PEG-PA/DM coating seems further to enhance Cu-LDH tumor accumulation, revealing that PEG on the Cu-LDH NP surface helps more efficiently reduce the clearance by the liver and spleen, and accumulate in the tumor tissue.

We further summarized the biodistribution of naked or modified LDH NPs reported by other researchers (Table 1),[20,34,35] which seemed to effectively accumulate at the tumor sites. However, these data may not be so reliable because (1) there is an abundance of Mg as well as Al in each organ, so the determined Mg/Al biodistributions do not reflect the LDH NP biodistribution; and (2) the carried drug may be released during circulation, so its biodistribution may not truly represent the LDH NP biodistribution. Thus, the comparison with these reported data is not so meaningful. In our research, the trace element (Cu) was chosen, which most likely represents LDH NP biodistribution because Cu ions are strongly associated with LDH NPs and the Cu body level is relatively low.

## CONCLUSIONS

In summary, we have developed a strategy to stabilize LDH nanoparticles with charge-convertible polymer PAMA/DMMA and increase their tumor accumulation for potential tumor therapy. The surface of LDH NPs was coated with a negatively charged PAMA/DMMA polymer via electrostatic interaction, which made Cu-LDH@PAMA/DMMA nanohybrids well dispersed in electrolyte solutions for steady circulation in blood. Once in a weakly acidic environment, charge conversion of the polymer via hydrolysis re-exposed positively charged LDH NPs to facilitate cancer cell internalization and subsequent therapy. The PAMA/DMMA coating on Cu-LDH NPs also reduced the nonspecific capture in normal tissues (such as live and spleen) but facilitated their accumulation in the weakly acidic tumor microenvironment. This work thus provides a way to modify positively charged nanomaterials to improve tumor accumulation for safe and effective delivery of anticancer drug/gene in vivo.

## EXPERIMENTAL SECTION

**Preparation of Cu-LDH.** Fresh precursor $Mg_3Al$-LDH suspension (20 mL; ~8 mg/mL) was prepared according to our previous work.[36] Then, $CuCl_2$ solution (40 mL, 10 mM) was added slowly to 1 mL of $Mg_3Al$-LDH (8 mg/mL) suspension with vigorous stirring. After 6 h stirring, the Cu-LDH was collected via centrifugation and washed three times with water. The obtained slurry Cu-LDH was dispersed in deionized water manually, which became homogeneously dispersed at room temperature after occasionally shaking for 1−2 days.

**Synthesis of PAMA.** Briefly, ethyl $\alpha$-bromoisobutyrate (19.5 mg, 14 $\mu$L), 2-aminoethyl methacrylate (AMA) hydrochloride (1.65 g), and 2,2′-bipyridyl (31.2 mg) were dissolved in dimethylformamide and $H_2O$ mixture and then bubbled with $N_2$ at room temperature for 20 min. Then, copper(I)



https://dx.doi.org/10.1021/acsomega.0c05520
ACS Omega 2021, 6, 3822−3830

chloride (9.9 mg) was added to the reaction mixture and stirred under $N_2$ for another 10 min. After 24 h stirring at 60 °C in an oil bath, the reaction mixture was dialyzed against water (molecular weight cutoff (MWCO), 1000 Da). The final product was acquired through a freeze-drying process.

**Synthesis of PAMA/DMMA.** PAMA (235 mg) was dissolved in water, and 0.1 M NaOH solution was added to adjust the solution pH to 8.5. 2,3-Dimethylmaleic anhydride (530 mg) was divided into three parts and added to the above solution three times. After stirring overnight, the mixture was purified in a dialysis bag (MWCO, 3500 Da) and PAMA/DMMA finally lyophilized.

**Preparation of Cu-LDH@PAMA/DMMA.** The Cu-LDH suspension (1 mL, 1 mg/mL) was dropwise added to 3 mL of PAMA/DMMA aqueous solution (1 mg/mL) under vigorous stirring, which was stirred for another 4 h. The final Cu-LDH@PAMA/DMMA hybrid was collected via centrifugation and then redispersed in aqueous solutions. The coating of Cu-LDH with a varied amount of PAMA/DMMA was also investigated similarly.

**Characterization.** The morphology and microstructure of LDH nanoparticles were analyzed using transmission electron microscopy (TEM, HITACHI 7700) operated at 80 kV. The powder X-ray diffraction (XRD) pattern of freeze-dried samples was recorded on a Rigaku Miniflex X-ray diffractometer using Cu K$\alpha$ radiation at a scanning rate of 5°/min. The Fourier transform infrared (FT-IR) spectrum of freeze-dried samples was obtained using a Nicolet 5700 FT-IR spectrometer (Thermo Electron Corporation) at a resolution of 4 $cm^{-1}$ for 32 scans. The quantitative Cu, Mg, and Al contents in samples or in tissues were determined using inductively coupled plasma-optical emission spectrometry (ICP-OES) or inductively coupled plasma-mass spectrometry (ICP-MS) on a Varian Vista Pro instrument. Cu-LDH@PAMA/DMMA (100 $\mu$L, 4 mg/mL) was mixed with 900 $\mu$L of HEPES buffer (20 mM, pH 7.4 or 6.8) and then the mixture was shaken for 2 h at 37 °C. The hydrodynamic average size and the $\zeta$-potential of these LDH-based nanohybrids were measured using dynamic light scattering (DLS, Malvern).

For assessing the longitudinal relaxivity ($r_1$), Cu-LDH nanoparticles were dispersed into two buffers with pH 7.4 and 6.0, respectively. Then, the heterogeneous buffer suspensions were shaken for 1 h at 37 °C with a speed of 100 rpm in a water bath and mixed with agarose buffer solution (1%, fixing agent) with the corresponding pH value in SampleJet tubes (5.0 × 103.5 $mm^2$, Bruker) for MRI scanning.

**Confocal Fluorescence Microscopy Imaging of Cellular Uptake.** Macrophages (Raw 264.7) and B16F0 cancer cells were cultured in a complete Dulbecco's modified Eagle's medium (DMEM) including 10% fetal bovine serum and 1% penicillin/streptomycin and then incubated in a 37 °C incubator supplying 5% $CO_2$. Raw 264.7/B16F0 cells were seeded on a coverslip in a 24-well plate at a density of 5 × $10^4$ cell/well and incubated overnight to allow cell attachment. Then, the cells were treated with a fresh medium with pH 7.4 or 6.8 that contained Cu-LDH@PAMA/DMMA (100 $\mu$g/mL FITC/Cu-LDH, 10 $\mu$g/mL FITC, 15 $\mu$g/mL Cu) and incubated for another 4 h. After washing three times with PBS and nucleus staining with DAPI, the confocal images were recorded in a Leica SP8 confocal LSM.

**Flow Cytometry Analysis of Cellular Uptake.** Raw 264.7/B16F0 cells were seeded in a 12-well plate at a density of 1 × $10^5$ cell/well and incubated overnight to allow cell attachment. Then, the cells were treated with a fresh medium with pH 7.4 or 6.8 that contained Cu-LDH@PAMA/DMMA (50 $\mu$g/mL FITC/Cu-LDH, 5 $\mu$g/mL FITC, 7.5 $\mu$g/mL Cu) and incubated for another 4 h at 37 °C. The cells were detached from the well via adding trypsin-EDTA and collected in a vial. After washing with PBS for three times, the cell fluorescence intensity was measured in CytoFLEX (Beckman, IN).

**Photothermal Conversion Evaluation.** Cu-LDH and Cu-LDH@PAMA/DMMA solution (1 mL, [Cu] = 125 $\mu$g/mL) were put in a quartz cuvette and then exposed to an 808 nm laser at a power density of 1.0 W/cm for 5 min. The temperature profiles were recorded using a FLIR ONE infrared thermal camera.

**Cell Viability Assay.** B16F0 cells were seeded in a 48-well plate at a density of 1 × $10^4$ cell/well in 200 $\mu$L of culture medium. After 24 h incubation at 37 °C, the cells were treated with various Cu-LDH formulations. For the laser treatment group, the medium was replaced with a fresh one, the cells were irradiated with the 808 nm laser (1 W/$cm^2$, 5 min) after 20 h uptake and washing away of nanoparticles three times, and then the group was incubated in standard medium for another 4 h. For groups without laser treatment, the cells were continuously incubated for 24 h. Then, the cell viability was examined by the 3-(4, 5-dimethylthiazol-2-yl)-2,5diphenyltetrazolium bromide (MTT) assay.

***In Vivo* MRI Imaging to Determine Cu-LDH Tumor Accumulation.** The melanoma tumor model was built by implanting subcutaneously 1 × $10^5$ B16F0 cells on the right back of each mouse. All animal procedures were carried out in accordance with the guidelines of the Animal Ethics Committee of Hainan Medical University. After the tumor diameter reached ∼6-8 mm, each mouse was iv-injected with 100 $\mu$L of Cu-LDH@PAMA/DMMA containing 20 $\mu$g of Cu (i.e., 1 mg/kg of Cu). The $T_1$-weighted MR (Bruker Biospin, Karlsruhe, Germany) images were recorded at 0, 2, 4, 8 24, 48, and 72 h postinjection using FOV (field of view) = 30 × 30 $mm^2$, MTX (matrix size) = 128 × 128, TR/TE (reception time/echo time) = 400.0/5.5 ms, FA (flip angle) = 90°, and slice thickness = 1 mm.

**Biodistribution of Cu-LDH@PAMA/DMMA.** Three B16F0-bearing C57BL/6 mice were iv-injected with Cu-LDH@PAMA/DMMA at a dose of 1 mg/kg of Cu. After 24 h injection, the mice were sacrificed and major organs (heart, liver, spleen, lung, kidney, tumor) were harvested for ICP-MS (Varian Vista Pro) analysis of the Cu amount.

**Statistical Analysis.** All experiments were performed at least in triplicate with the data expressed as the mean ± standard deviation. Two-way analysis of variance (two-way ANOVA) and Student's *t*-test were used to test significant differences between the experimental groups. NS, no significant difference when $p > 0.05$, *$p < 0.05$, **$p < 0.01$, ***$p < 0.001$, and ****$p < 0.0001$.

## ■ ASSOCIATED CONTENT

### Supporting Information

The Supporting Information is available free of charge at https://pubs.acs.org/doi/10.1021/acsomega.0c05520.

Polymer (PAMA/DMMA) charge conversion mechanism and synthesis route; NMR of polymers PAMA and PAMA/DMMA; UV−vis absorption, photothermal conversion, stability, and efficiency of Cu-LDH nano-



https://dx.doi.org/10.1021/acsomega.0c05520
ACS Omega 2021, 6, 3822−3830

particle suspension; colloidal stability of Cu-LDH@PAMA/DMMA nanoparticles in PBS and DMEM; and time-dependent cellular uptake (PDF)

## AUTHOR INFORMATION


### Corresponding Authors

**Zhi Ping Xu** − *Australian Institute for Bioengineering and Nanotechnology (AIBN), The University of Queensland, St. Lucia, QLD 4072, Australia;* orcid.org/0000-0001-6070-5035; Email: gordonxu@uq.edu.au

**Qing Sun** − *Department of Pathology, Shandong Provincial Qianfoshan Hospital, Cheeloo College of Medicine, Shandong University, Jinan, Shandong Province 250014, People's Republic of China; Department of Pathology, The First Affiliated Hospital of Shandong First Medical University & Shandong Provincial Qianfoshan Hospital, Jinan, Shandong Province 250014, People's Republic of China;* Email: qingsw99@sdhospital.com.cn

### Authors

**Tiefeng Xu** − *Department of Pathology, Shandong Provincial Qianfoshan Hospital, Cheeloo College of Medicine, Shandong University, Jinan, Shandong Province 250014, People's Republic of China; The First Affiliated Hospital and The Oncological Institute of Hainan Medical University, Haikou City, Hainan Province 570102, People's Republic of China*

**Jianping Liu** − *Australian Institute for Bioengineering and Nanotechnology (AIBN), The University of Queensland, St. Lucia, QLD 4072, Australia*

**Luyao Sun** − *Australian Institute for Bioengineering and Nanotechnology (AIBN), The University of Queensland, St. Lucia, QLD 4072, Australia*

**Run Zhang** − *Australian Institute for Bioengineering and Nanotechnology (AIBN), The University of Queensland, St. Lucia, QLD 4072, Australia;* orcid.org/0000-0002-0943-824X

Complete contact information is available at: https://pubs.acs.org/10.1021/acsomega.0c05520

### Author Contributions

‖T.X. and J.L. contributed equally to this work.


### Notes

The authors declare no competing financial interest.

## ACKNOWLEDGMENTS

This research is financially supported by the Key International Co-operation Project of the Department of Science and Technology of Hainan Province (Grant No. ZDYD2019205), Australian Research Council (ARC) Discovery Project (DP190103486), and Shandong Provincial Major Scientific and Technological Innovation Project (No. 2019JZZY010108). The authors further appreciate the facilities and the technical assistance of the Australian Microscopy & Microanalysis Research Facility at the Centre for Microscopy and Microanalysis (CMM), Australian National Fabrication Facility (ANFF), and Centre of Advanced Imaging (CAI), The University of Queensland.

## REFERENCES

(1) Cheng, L.; Wang, X.; Gong, F.; Liu, T.; Liu, Z. 2D Nanomaterials for cancer theranostic applications. *Adv. Mater.* **2020**, *32*, No. 1902333.

(2) Yang, K.; Feng, L.; Hong, H.; Cai, W.; Liu, Z. Preparation and functionalization of graphene nanocomposites for biomedical applications. *Nat. Protoc.* **2013**, *8*, 2392−2403.

(3) Kalantar-Zadeh, K.; Ou, J. Z.; Daeneke, T.; Strano, M. S.; Pumera, M.; Gras, S. L. Two-dimensional transition metal dichalcogenides in biosystems. *Adv. Funct. Mater.* **2015**, *25*, 5086−5099.

(4) Luo, M.; Fan, T.; Zhou, Y.; Zhang, H.; Mei, L. 2D black phosphorus−based biomedical applications. *Adv. Funct. Mater.* **2019**, *29*, No. 1808306.

(5) Xu, M.; Yang, G.; Bi, H.; Xu, J.; Dong, S.; Jia, T.; Wang, Z.; Zhao, R.; Sun, Q.; Gai, S.; He, F.; Yang, D.; Yang, P. An intelligent nanoplatform for imaging-guided photodynamic/photothermal/chemo-therapy based on upconversion nanoparticles and CuS integrated black phosphorus. *Chem. Eng. J.* **2020**, *382*, No. 122822.

(6) Cao, Z.; Li, B.; Sun, L.; Li, L.; Xu, Z. P.; Gu, Z. 2D layered double hydroxide nanoparticles: recent progress toward preclinical/clinical nanomedicine. *Small Methods* **2019**, *4*, No. 1900343.

(7) Wang, Z.; Zhu, H.; He, F.; Yan, D.; Jia, T.; Sun, Q.; Wang, X.; Wang, X.; Yang, D.; Gai, S.; Yang, P. Layer structured LDH_ZnPcG4-FA nanoplatform for targeted and imaging guided chemo-photodynamic therapy mediated by 650 nm light. *Chem. Eng. J.* **2020**, *382*, No. 122847.

(8) Xu, M.; Wei, M. Layered double hydroxide-based catalysts: recent advances in preparation, structure, and applications. *Adv. Funct. Mater.* **2018**, *28*, No. 1802943.

(9) Oh, J. M.; Choi, S. J.; Lee, G. E.; Kim, J. E.; Choy, J. H. Inorganic metal hydroxide nanoparticles for targeted cellular uptake through clathrin-mediated endocytosis. *Chem. - Asian J.* **2009**, *4*, 67−73.

(10) Bae, Y. H.; Park, K. Targeted drug delivery to tumors: myths, reality and possibility. *J. Controlled Release* **2011**, *153*, 198−205.

(11) Muráth, S.; Szerlauth, A.; Sebk, D.; Szilágyi, I. Layered double hydroxide nanoparticles to overcome the hydrophobicity of ellagic acid: an antioxidant hybrid material. *Antioxidants* **2020**, *9*, No. 153.

(12) Somosi, Z.; Muráth, S.; Nagy, P.; Sebők, D.; Szilagyi, I.; Douglas, G. Contaminant removal by efficient separation of in situ formed layered double hydroxide compounds from mine wastewaters. *Environ. Sci. Water Res. Technol.* **2019**, *5*, 2251−2259.

(13) Cao, Z.; Adnan, N. N. M.; Wang, G.; Rawal, A.; Shi, B.; Liu, R.; Liang, K.; Zhao, L.; Gooding, J. J.; Boyer, C.; Gu, Z. Enhanced colloidal stability and protein resistance of layered double hydroxide nanoparticles with phosphonic acid-terminated PEG coating for drug delivery. *J. Colloid Interface Sci.* **2018**, *521*, 242−251.

(14) Gu, Z.; Zuo, H.; Li, L.; Wu, A.; Xu, Z. P. Pre-coating layered double hydroxide nanoparticles with albumin to improve colloidal stability and cellular uptake. *J. Mater. Chem. B* **2015**, *3*, 3331−3339.

(15) Li, L.; Gu, W.; Liu, J.; Yan, S.; Xu, Z. P. Amine-functionalized $SiO_2$ nanodot-coated layered double hydroxide nanocomposites for enhanced gene delivery. *Nano Res.* **2015**, *8*, 682−694.

(16) Kura, A. U.; Hussein-Al-Ali, S. H.; Hussein, M. Z.; Fakurazi, S. Preparation of tween 80-Zn/Al-levodopa-layered double hydroxides nanocomposite for drug delivery system. *Sci. World J.* **2014**, *2014*, No. 104246.

(17) Pavlovic, M.; Rouster, P.; Somosi, Z.; Szilagyi, I. Horseradish peroxidase-nanoclay hybrid particles of high functional and colloidal stability. *J. Colloid Interface Sci.* **2018**, *524*, 114−121.

(18) Zhang, Y.; Wu, X.; Li, H.; Du, N.; Song, S.; Hou, W. Preparation and characterization of (betamethasone sodium phosphate intercalated layered double hydroxide)@liposome nanocomposites. *Colloid Surf., A* **2017**, 824−831.

(19) Yan, M.; Zhang, Z.; Cui, S.; Zhang, X.; Zhao, C.; et al. Preparation and evaluation of PEGylated phospholipid membrane coated layered double hydroxide nanoparticles. *Asian J. Pharm. Sci.* **2016**, *11*, 396−403.

(20) Ray, S.; Saha, S.; Sa, B.; Chakraborty, J. In vivo pharmacological evaluation and efficacy study of methotrexate-encapsulated polymer-coated layered double hydroxide nanoparticles for possible application in the treatment of osteosarcoma. *Drug Delivery Transl. Res.* **2017**, *7*, 259−275.

(21) Somosi, Z.; Pavlovic, M.; Pálinkó, I.; Szilágyi, I. Effect of polyelectrolyte mono- and bilayer formation on the colloidal stability of layered double hydroxide nanoparticles. *Nanomaterials* **2018**, *8*, No. 986.
(22) Pavlovic, M.; Náfrádi, B.; Rouster, P.; Muráth, S.; Szilagyi, I. Highly stable enzyme-mimicking nanocomposite of antioxidant activity. *J Colloid Interface Sci.* **2019**, *543*, 174−182.
(23) van Meer, G.; Voelker, D. R.; Feigenson, G. W. Membrane lipids: where they are and how they behave. *Nat. Rev. Mol. Cell Biol.* **2008**, *9*, 112−24.
(24) Xu, Z. P.; Niebert, M.; Porazik, K.; Walker, T. L.; Cooper, H. M.; Middelberg, A. P. J.; Gray, P. P.; Bartlett, P. F.; Lu, G. Q. Subcellular compartment targeting of layered double hydroxide nanoparticles. *J. Controlled Release* **2008**, *130*, 86−94.
(25) Li, S.; Zhao, Z.; Wu, W.; Ding, C.; Li, J. Dual pH-responsive micelles with both charge-conversional property and hydrophobic-hydrophilic transition for effective cellular uptake and intracellular drug release. *Polym. Chem.* **2016**, *7*, 2202−2208.
(26) Chu, Z.; Wang, Z.; Chen, L.; Wang, X.; Huang, C.; Cui, M.; Yang, D.-P.; Jia, N. Combining magnetic resonance imaging with photothermal therapy of CuS@BSA nanoparticles for cancer theranostics. *ACS Appl. Nano Mater.* **2018**, *1*, 2332−2340.
(27) Ge, R.; Lin, M.; Li, X.; Liu, S.; Wang, W.; Li, S.; Zhang, X.; Liu, Y.; Liu, L.; Shi, F.; Sun, H.; Zhang, H.; Yang, B. $Cu^{2+}$-loaded polydopamine nanoparticles for magnetic resonance imaging-guided pH- and near-infrared-light-stimulated thermochemotherapy. *ACS Appl. Mater. Interfaces* **2017**, *9*, 19706−19716.
(28) Pan, D.; Caruthers, S. D.; Senpan, A.; Yalaz, C.; Stacy, A. J.; Hu, G.; Marsh, J. N.; Gaffney, P. J.; Wickline, S. A.; Lanza, G. M. Synthesis of NanoQ, a copper-based contrast agent for high-resolution magnetic resonance imaging characterization of human thrombus. *J. Am. Chem. Soc.* **2011**, *133*, 9168−9171.
(29) Liu, Y.; Wu, J.; Jin, Y.; Zhen, W.; Wang, Y.; Liu, J.; Jin, L.; Zhang, S.; Zhao, Y.; Song, S.; Yang, Y.; Zhang, H. Copper(I) phosphide nanocrystals for in situ self-generation magnetic resonance imaging-guided photothermal-enhanced chemodynamic synergetic therapy resisting deep-seated tumor. *Adv. Funct. Mater.* **2019**, *29*, No. 1904678.
(30) Li, B.; Tang, J.; Chen, W.; Hao, G.; Kurniawan, N.; Gu, Z.; Xu, Z. P. Novel theranostic nanoplatform for complete mice tumor elimination via MR imaging-guided acid-enhanced photothermo-/chemo-therapy. *Biomaterials* **2018**, *177*, 40−51.
(31) Kluger, R.; Chin, J.; Choy, W. Carboxylic acid participation in amide hydrolysis. Reactivity of intermediates in the internally catalyzed hydrolysis of n-Substituted 2, 3-dimethylmaleamic acids. *J. Am. Chem. Soc.* **1979**, *101*, 6976−6980.
(32) Liu, J.; Wu, Y.; Fu, C.; Li, B.; Li, L.; Zhang, R.; Xu, T.; Xu, Z. P. Charge reversion simultaneously enhances tumor accumulation and cell uptake of layered double hydroxide nanohybrids for effective imaging and therapy. *Small* **2020**, *16*, No. 2002115.
(33) Shi, S.; Fliss, B. C.; Gu, Z.; Zhu, Y.; Hong, H.; Valdovinos, H. F.; Hernandez, R.; Goel, S.; Luo, H.; Chen, F.; et al. Chelator-free labeling of layered double hydroxide nanoparticles for in vivo PET imaging. *Sci. Rep.* **2015**, *5*, No. 16930.
(34) Gao, R.; Mei, X.; Yan, D.; Liang, R.; Wei, M. Nano-photosensitizer based on layered double hydroxide and isophthalic acid for singlet oxygenation and photodynamic therapy. *Nat. Commun.* **2018**, *9*, No. 2798.
(35) Choi, S.-J.; Oh, J.-M.; Choy, J.-H. Biocompatible nanoparticles intercalated with anticancer drug for target delivery: pharmacokinetic and biodistribution study. *J. Nanosci. Nanotechnol.* **2010**, *10*, 2913−2916.
(36) Li, B.; Gu, Z.; Kurniawan, N.; Chen, W.; Xu, Z. P. Manganese-based layered double hydroxide nanoparticles as a $T_1$-MRI contrast agent with ultrasensitive pH response and high relaxivity. *Adv. Mater.* **2017**, *29*, No. 1700373.


https://dx.doi.org/10.1021/acsomega.0c05520
*ACS Omega* 2021, 6, 3822−3830